JAAS

PAPER

Cite this: *J. Anal. At. Spectrom.*, 2018, **33**, 835

Multi-element analysis of single nanoparticles by ICP-MS using quadrupole and time-of-flight technologies†

Steffi Naasz,[a] Stefan Weigel,‡[a] Olga Borovinskaya,[b] Andrius Serva,[c] Claudia Cascio,§[a] Anna K. Undas,[a] Felice C. Simeone,¶[a] Hans J. P. Marvin[a] and Ruud J. B. Peters*[a]

Determining composition, shape, and size of nanoparticles dispersed in a complex matrix is necessary in the assessment of toxicity, for regulatory actions, and environmental monitoring. Many types of nanoparticles that are currently used in consumer products contain more than one metal which are often not uniformly distributed (*e.g.*, core–shell nanoparticles). This compositional and structural complexity makes their characterization difficult. In this study, we investigate the capability of single particle inductively coupled plasma mass spectrometry (spICP-MS) using time-of-flight (TOF) and quadrupole (Q) mass analyzers to determine the composition, size distribution, and concentration of a series of nanoparticles that are used in a variety of industrial applications: $BiVO_4$, $(Bi_{0.5}Na_{0.5})TiO_3$ and steel (which contains Fe, Cr, Ni, Mo) nanoparticles. In addition, we tested both types of mass analyzers with Au-core/Ag-shell nanoparticles, which are well-characterized and have already been used for assessment of multi-element capabilities of spICP-MS. The results confirm that both types of mass analyzers produce accurate estimations of the size of Au-core/Ag-shell particles. For other multi-element nanoparticles, spICP-MS provided the size of aggregates and/or agglomerates in the prepared suspensions. In general, particle size detection limits (d_{LOD}) of spICP-TOFMS instruments with values of 29 nm for Ti, 14 nm for Mo, and 7 nm for Au, are smaller than those obtained for the quadrupole instruments. This study finds that only spICP-TOFMS can accurately assess the elemental composition of nano-steel particles. By contrast, spICP-QMS is limited to the detection of 2 elements in an individual particle and the elemental composition of nano-steel particles is less accurate. In general, spICP-TOFMS was able to quantify multiple elements with high precision and that currently makes it the first choice for multi-element detection of unknown nanoparticles.

Received 4th December 2017
Accepted 17th April 2018

DOI: 10.1039/c7ja00399d

rsc.li/jaas

1. Introduction

Determining the chemical composition of nanoparticles (NPs) is crucial in toxicological and environmental studies, regulatory control and quality assessment. While the analysis of nanoparticles composed of a single element by using single particle inductively coupled plasma mass spectrometry (spICP-MS) has reached reliable standards,[1–4] the determination of size, composition and concentration of nanoparticles composed of multiple elements (*e.g.*, nanocomposites) remains challenging. Multi-element nanoparticles represent a substantial portion of manufactured materials and they are used as additives in a wide variety of common commercial goods such as food and cosmetics.[3] Often the complexity of the matrix in which these nanoparticles are embedded complicates their analysis further.[5] Recent studies have explored the multi-element capability of spICP-MS by using a prototype time-of-flight (TOF) mass spectrometer, which can analyze multiple elements simultaneously,[6] or by using a quadrupole (Q) mass spectrometer, which can analyze multiple elements in ultra-fast scanning mode.[7]

TOF mass analyzers extract short packages of ions and send them to a field-free-region, where they separate according to their velocity, and their arrival times are registered at the detector. The main advantage of a TOF mass analyzer is the

[a]*RIKILT, Wageningen University & Research, Akkermaalsbos 2, 6708 WB Wageningen, The Netherlands. E-mail: ruudj.peters@wur.nl*

[b]*TOFWERK, Uttigenstrasse 22, CH-3600 Thun, Switzerland*

[c]*Fluidigm Corp., 7000 Shoreline Court, South San Francisco, CA 94080, USA*

† Electronic supplementary information (ESI) available: ESI on the instrument specifics reported by the manufacturers (Table S1), parameters for spICP-MS measurements (Tables S2–S5), nanoparticle characteristics (Table S6, Fig. S1), particle size distributions of all particles involved in this study (Fig. S2), temporal shifts of Ti and Bi signals (Fig. S3) and distribution histogram of V/Bi and Ti/Bi molar ratios (Fig. S4). See DOI: 10.1039/c7ja00399d

‡ Current address: BfR – Federal Institute for Risk assessment, Max-Dohrn-Strasse 8-10, 10589 Berlin, Germany.

§ Current address: EFSA – European Food Safety Authority, Via Carlo Magno, 1A, 43126 Parma PR, Italy.

¶ Current address: ISTEC – Institute of Science and Technology of Ceramic Materials, Via Granarolo 64-48018 Faenza, Italy.

acquisition of a full mass spectrum within a short time period.[8] In an ICP-QMS instrument, oscillating electric fields separate ions traveling through the space between four electrodes in a way that only ions with stable trajectories reach the detector. To detect different elemental isotopes, each characterized by a specific mass to charge (m/z) ratio, these fields must be adjusted rapidly.[9] Settling and dwell times of a quadrupole instrument are crucial parameters for an accurate analysis of nanoparticles. Dwell time is the time spent to measure a single m/z value and ranges from 10 μs for the fastest available quadrupole instruments[10] up to a few hundreds of milliseconds. The settling time is the time required by the quadrupole to stabilize for the measurement of the next m/z value.[11] Using short dwell and settling times (*i.e.*, μs range) makes it possible to detect at least two elements per particle, by recording 1–2 data point(s) per corresponding isotope.[7]

The majority of studies on composite nanoparticles have been conducted on core/shell particles, spherical nanoparticles with a non-uniform distribution of elemental components; Au within a core and Ag as shell-structure. These elements can be measured with a relatively high sensitivity and do not have many interferences.[6,12] Their behavior, however, cannot be generalized and extrapolated to any composite nanoparticle. Industrially relevant nanoparticles such as nano-steel (a Fe, Cr, Ni, Mo alloy used in composites), bismuth vanadate ($BiVO_4$, a widely used pigment due to its bright yellow color) and -sodium titanate ($(Bi_{0.5}Na_{0.5})TiO_3$, commonly used as ceramic materials) particles[13,14] investigated in this study challenge the spICP-MS method in more complex ways than Au or Ag based nanoparticles. This paper provides the first systematic and critical evaluation of the performance of ICP-TOFMS and -QMS instruments for the analysis of nanoparticles with complex structures and compositions.

2. Experimental section

2.1 Instruments

The instruments used in this study were two TOF instruments, the icpTOF (TOFWERK AG, Switzerland), and the CyTOF® 2 mass cytometer (Fluidigm Corp., USA), and two ICP-QMS instruments, the NexION® 350D (Perkin Elmer Scientific, USA), and the iCAP™ Q (Thermo Fisher Scientific, Germany). The icpTOF and CyTOF® 2 both combine a TOF mass analyzer with plasma chambers and ion optics similar to those used in conventional quadrupole ICP-MS.[8] These ICP-TOFMS instruments record 33.000 (icpTOF) and 76.800 (CyTOF® 2) mass spectra per second, yielding time resolutions of 30 μs and 13 μs, respectively (ESI Table S1†). Note that the CyTOF® 2 instrument has a limited mass range from 89–210 m/z, so acquisition of a "full-mass spectrum" within 13 μs is not accomplished. In general, the icpTOF instrument has a higher mass resolving power than the other instruments under investigation and that enables to resolve some polyatomic interferences. However, in this study we found that the use of H_2 as reaction gas is preferable to get the best detection limits for Fe (measuring $^{56}Fe^+$) and for Cr (measuring $^{52}Cr^+$) and this gas was therefore used for the nano-steel analysis.[15]

Regarding the quadrupoles, both instruments have a minimum dwell time of 100 μs in transient mode. The NexION® 350D can achieve a dwell time of 10 μs, but only within its Syngistix™ Nano Application Module, which, however, does not allow multi-element single particle measurements. In general, the settling time (*i.e.* the time between readings) is a parameter set by the manufacturer and cannot be adjusted by the user. The nominal settling time of the ICP-QMS is 120 μs in the NexION® 350D, and 75 μs in the iCAP™ Q. For sequential quantification of ions with large differences in atomic masses, the instrument can use longer settling times than the nominal. The listed settling times were confirmed experimentally. For further details of the instrument settings, see ESI Tables S2–S5.†

2.2 Materials

For multi-elemental analysis with both TOF and Q spICP-MS, we used the following materials (ESI Table S6, Fig. S1†):

Two types of spherical core–shell Au/Ag nanoparticles: (1) total diameter of 61 nm (Au/Ag 60) (KJW1905, 30 nm Au-core, 15 nm Ag-shell, concentration 0.021 g L^{-1}), and (2) 79 nm (Au/Ag 80) (KJW2242, 51 nm Au-core, 14 nm Ag-shell, concentration 0.021 g L^{-1}). For the analysis, we used suspensions of these materials in 2 mM citrate solutions (Nanocomposix, San Diego, USA). See ESI Fig. S1† for the SEM characterisation of this material.

Amorphous $BiVO_4$ particles (L. Boselli, University College Dublin (IRL)) with a median primary particle size of 69 nm ± 23 nm (as determined by SEM, ESI Fig. S1†). SEM images revealed the presence of aggregates/agglomerates.

Amorphous $(Bi_{0.5}Na_{0.5})TiO_3$ particles (L. Boselli, University College Dublin (IRL)) with a median primary particle size of 106 nm ± 49 nm (as determined by SEM, ESI Fig. S1†) and a broad size distribution. As with the previous material, SEM images revealed the presence of aggregates/agglomerates.

Composite nano-steel platelets (IRMM-383, composition as weight percentage: Fe 67–72%, Cr 16–26%, Ni 10–14%, Mo 2–4%). These platelets have thicknesses in the range of 20 to 30 nm, and lengths ranging from 100 to 1500 nm. SEM images revealed primary particle sizes of 192 ± 69 nm but also the presence of aggregates with sizes in the range 1–5 μm (ESI Fig. S1†). This nanomaterial was kindly provided by the EU NanoDefine project.

2.3 Analysis of particles by electron microscopy

Sizes and size distributions of the test particles were determined by scanning electron microscopy (SEM, FEI Magellan 400, FEI Company, USA). Droplets of the dispersion of nanoparticles were deposited on carbon foil covered stubs and dried at room temperature for 2 h. In order to increase the conductivity of the samples, a 5 nm iridium layer was deposited by inductive sputtering. The samples were imaged at an accelerating voltage of 10 kV and a working distance of ~5 mm. At least 150 individual primary particles were measured and the median primary particle size calculated assuming a spherical shape (ESI Table S6†). SEM images were edited and particle sizes were

measured with the help of Fiji, a plugin for the analysis of electron microscopy data.[16]

2.4 Preparation of suspensions of the test particles

In order to minimize the probability of detecting multiple particle events,[1] for each type of particle, dispersions containing $\sim 10^6$ particles mL^{-1} were prepared in Ultrapure Water (UPW, Millipore A10 system, Millipore, USA). The Au-core/Ag-shell, $(Bi_{0.5}Na_{0.5})TiO_3$, and $BiVO_4$ particles were provided in aqueous dispersions and were diluted further before each analysis. Suspensions of nano-steel particles were prepared from the powdered material according to a protocol of the NanoDefine project.[17] In short; 25 ± 2 mg of the nano-steel powder was weighted into a 50 mL polyethylene tube to which 10 mL of UPW was added to obtain a final mass concentration of 2.5 g L^{-1}. This suspension was vortexed for 2 min and sonicated for 10 min with a sonication probe (Misonix XL-2000, 3 mm probe, 4 W, Qsonica, USA) while cooled in an ice bath. The physicochemical properties of this material hamper the formation of a stable aqueous dispersion and the particles sediment rapidly due to their high density and relatively large size. The suspension was diluted to $\sim 10^6$ particles mL^{-1} and analyzed shortly after sonication to minimize the risk of particle sedimentation.

2.5 spICP-MS measurements and data analysis

Determination of particle size and particle number and mass concentration. The instrument settings of the ICP-TOFMS and ICP-QMS instruments used for the experiments are listed in the ESI (Tables S2–S5†). For measurements of size and concentrations, the QMS instruments were setup to monitor only one single isotope (the most suitable one was chosen). The TOFMS instruments measure all isotopes by default. A total runtime of 60 s and a dwell/integration time of 3 ms was used, with exception of the CyTOF® 2 instrument where 13 μs was used. Particle sizes and particle number and mass concentrations were calculated from the results of three independently prepared replicates of each type of nanoparticle and using an in-house developed single particle calculation tool.[18] This single particle calculation tool has been described in detail and validated in previous works.[19,20] In short, the recorded data from the ICP-QMS and ICP-TOFMS instruments are exported as a CSV-file and imported in the spreadsheet. Before analyses, the transport efficiency of the ICP-MS system was determined using a 50 ng L^{-1} suspension of 60 nm diameter Au nanoparticles (NIST RM8013) according to the method described by Pace *et al.* based on the certified particle size.[21] For the sizing of nanoparticles in suspension, ionic single-element standard solutions of Au, Ag, Ti, and Mo (Merck, 1 g L^{-1}), and a multi-element standard solution containing amongst others Bi, Fe, Ni and Cr (standard solution A, Merck, 10 mg L^{-1}) were used to determine the analyte response. The single particle calculation tool uses a frequency distribution to separate particle signals from dissolved material. The particle number concentration is determined from the observed number of particles in the time scan as follows:

$$C_p = \frac{N_p}{\eta_n} \times \frac{1000}{V} \quad (1)$$

where C_p = particle number concentration (L^{-1}); N_p = number of particles detected in the time scan (min^{-1}); η_n = transport efficiency; V = sample flow (mL min^{-1}). The mass of the individual particles is calculated as follows:

$$m_p = \frac{I_p t_d}{RF_{ion}} \times \frac{V \eta_n}{60} \times \frac{M_p}{M_a} \quad (2)$$

where m_p = particle mass (ng); I_p = particle signal intensity in time scan (cps); t_d = dwell time (s); RF_{ion} = ICP-MS response factor of analyte ion standard (cps μg^{-1} L^{-1}); M_p = molar mass nanoparticle material (g mol^{-1}); M_a = molar mass measured element (g mol^{-1}). The particle mass concentration is calculated as follows:

$$C_m = \frac{\sum m_p \times 1000}{\eta_n \times V \times t_a} \quad (3)$$

where C_m = particle mass concentration (ng L^{-1}); $\sum m_p$ = summed particle masses (ng) of particles detected in the time scan; η_n = transport efficiency; V = sample flow (mL min^{-1}); t_a = duration of time scan (min). The particle size, expressed as the spherical equivalent diameter, is calculated as follows:

$$d_p = \sqrt[3]{\frac{6m_p}{\pi \rho_p}} \times 10^4 \quad (4)$$

where dp = spherical equivalent diameter of the particle (nm); ρ_p = bulk density of the particle (g mL^{-1}). The bulk densities used for the materials in this study were as follows: Au 19.3, Ag 10.5, $(Bi_{0.5}Na_{0.5})TiO_3$ 5.9, $BiVO_4$, 7.0 g mL^{-1}. For Au-core/Ag-shell particles, the Ag-shell thickness of individual particles was calculated as follows:

$$r_{Ag_{shell}} = \sqrt[3]{\frac{3\left(\left(\frac{m_{Au}}{\rho_{Au}}\right) + \left(\frac{m_{Ag}}{\rho_{Ag}}\right)\right)}{4\pi}} \times 10^4 - \frac{d_{Au_{core}}}{2} \quad (5)$$

where $r_{Ag_{shell}}$ = Ag-shell thickness (nm); m_{Au} and m_{Ag} = particle mass as determined with eqn (2) (ng); ρ_{Au} and ρ_{Ag} are the bulk densities of Au and Ag (g mL^{-1}); $d_{Au_{core}}$ = particle diameter as determined with eqn (4) (nm). All calculations were based on the detection of at least 100 particles per run.

Determination of the limit of detection for particle size. The limit of detection for size (d_{LOD}) is often calculated assuming a normal distribution of ion intensity from the blank using 3× sigma (which is accurate for high number of counts). The threshold for particle signals is often defined as $\mu + 3\sigma$, where μ and σ are the mean and the standard deviation of the intensity distribution of dissolved ions in the sample and instrument noise.[22] However, for a low number of counts, the noise is better described by Poisson distribution, in which case the variance equals the average of the squared differences from the mean number of counts, leading to detection mass limit of a particle given by:[6,23,24]

$$m_{LOD} = \frac{3.29 \times \sqrt{I_b \times t_b} + 2.72}{RF_{ion} \times t_d} \times \frac{V \eta_n}{60} \times \frac{M_p}{M_a} \quad (6)$$

where m_{LOD} = mass of the smallest particle that can be detected (ng); I_b = the mean of the background signal in the time scan (cps); 2.72 is an empirically determined constant.[23,24] Finally, based on the m_{LOD} the corresponding d_{LOD} (nm) is calculated using eqn (4). The instruments were optimized to decrease d_{LOD} using the collision/reaction cell (KED/CCT) mode with either helium (iCAP™ Q, NexION® 350D) as collision gas, or hydrogen (icpTOF) as reaction gas (ESI Tables S2–S5†). This option was not available for the CyTOF® 2 instrument, which, therefore, was used in standard mode only. LOD values are also influenced by the choice of isotope ion to be monitored, *e.g.* $^{48}Ti^+$ (73.8%) *versus* $^{47}Ti^+$ (7.3%) *etc.* (isotopic abundances in parentheses). While isotopes of higher abundance usually give better sensitivity, they may suffer more from interferences which increase the background intensity. Best isotopes were chosen for the measurement based on evaluation of the optimal signal-to-noise ratio of all isotopes ESI Tables S2–S5.†

Calculation of the percentage of multi-element particle events per run. To determine the multi-element detection capability, the instruments were operated in transient mode and the signals of the elements of interest were determined simultaneously at integration times of 30 μs and 13 μs for the icpTOF and CyTOF 2 instruments, respectively, and in rapid succession with dwell times of 100 μs for the ICP-QMS instruments. We estimated the multi-element capability of TOFMS and QMS instruments by counting the number of events with two or more isotopes detected relative to the total number of events in which a particle was detected. The signal was considered to be a particle if the intensity of at least one isotope was above the detection limit. In addition, the time-resolved multi-element detection of the icpTOF instrument was used to estimate the width of transient signals generated by single nanoparticles (TofViewer Software from Tofwerk).

Calculation of elemental composition of nano-steel. For the icpTOF instrument, the mass of each element in every individual particle was determined and the corresponding mass fraction of each element (X) was calculated using 100% normalization. Only particles with all four isotopes above LODs were considered for this evaluation and average and standard deviation of mass fractions calculated from 2000 particles are reported. Quantitative detection of multiple isotopes in individual steel particles with QMS was not feasible due to limitation of the technique. Therefore, the same calculation as for the icpTOF instrument was performed for the QMS instruments, but not on the single particle basis. Instead, element masses and mass fractions were calculated from average particle signal intensity of the entire population.

3. Results and discussion

3.1 Determination of particle size and size distribution

Au-core/Ag-shell particles. The results of the spICP-MS analysis of the Au-core/Ag-shell particles are presented in Table 1 and show that the sizes of both particles as determined with ICP-MS are close to the values determined with SEM and to the values reported by the supplier. Note that in these particle size analyses by ICP-QMS the isotopes of Au and Ag were measured in two separate runs, as oppose to TOFMS where all isotopes are acquired simultaneously. For the Au/Ag 60 particle, all four ICP-MS systems determine an average thickness of the Ag shell of ~11 nm, while the value reported by the supplier is 15 nm. By contrast, the thickness determined for the Ag-shell of the Au/Ag 80 particle (~13 nm) is in closer agreement with that reported by the supplier (14 nm). For the total diameter and the diameter of the Au-core, both Q- and TOF-ICP-MS systems showed comparable results which did not differ significantly from the values determined by SEM (Table 1) with two exceptions. For the Au/Ag 60 particle the CyTOF® 2 showed a size of the Au-core (26 nm ± 1 nm) that was ~4 nm smaller than the SEM value reported by the supplier (30 nm ± 3 nm) and the NexION® 350D produced an Au-core size 7 nm larger (37 nm ± 1 nm). However, these differences are not statistically

Table 1 Median particle sizes (mean) ± average standard deviation or particle size range (in brackets) determined by spICP-MS (calculated as equivalent to spherical diameters). The error represents the average standard deviation of the standard deviation of the size distribution in 3 independent runs

		Particle size determined by spICP-MS (nm)			
Nanoparticle type	Primary particle size (nm)	icpTOF	CyTOF® 2	NexION® 350D	iCAP™ Q
Au/Ag 60					
Total diameter	57 ± 5[a]				
Core diameter	30 ± 3[b]	30 ± 7	26 ± 10	37 ± 6	30 ± 6
Shell thickness	15[b]	11 ± 4	10 ± 5	11 ± 3	11 ± 3
Au/Ag 80					
Total diameter	80 ± 5[a]				
Core diameter	51 ± 6[b]	50 ± 14	56 ± 11	52 ± 9	49 ± 8
Shell thickness	14[b]	13 ± 4	13 ± 3	12 ± 3	12 ± 3
$BiVO_4$	69 ± 23[a]	178 (95–650)	194 (100–500)[c]	188 (115–1400)	197 (130–990)
$(Bi_{0.5}Na_{0.5})TiO_3$	106 ± 49[a]	162 (85–520)	164 (100–510)[c]	221 (95–970)	160 (70–635)
Nano-steel	197 ± 89[a]	355 (180–1600)	—	384 (205–2400)	380 (186–1600)

[a] Determined by SEM. [b] SEM/TEM value reported by the particle supplier. [c] Calculated based on isotope ^{209}Bi only.

significant when the standard deviations of the size distributions are taken into account. The average standard deviation given in Table 1 is the average of the standard deviations in the size distributions of each analysis ($n = 3$) and not the average of the mean particle size. The size distributions of the Au-core/Ag-shell particles are presented in the ESI (Fig. S2†) and show more or less symmetrical peak shapes around the median particle size, comparable to the peak shapes of the particles in EM analysis (ESI Fig. S1†). In an excellent review paper Montano *et al.* explain the shape of these size distributions as resulting from the polydispersity of the droplets generated by the nebulizer and entering the plasma.[25] Large droplets will complete desolvation farther downstream in the plasma than small droplets and therefore nanoparticle vaporization will begin farther downstream the plasma. The resulting ion cloud will have less time to diffuse before reaching the sampling orifice compared with ions produced from a nanoparticle that was carried into the plasma in a smaller droplet. This will introduce some variation in the intensity and duration of the ICP-MS signals from nanoparticles of the same size resulting in a broadening of the peak shape. It is interesting to see that different sized particles, *i.e.* the Au/Ag 60 and 80 particles, give the correct particle size which is an indication that the transport efficiency is similar for different sized particles. This was already confirmed by another study by Peters *et al.*, where different sized Au, Ag, TiO_2 and SiO_2 particles were analysed using spICP-MS and linear particle size ranges were established.[19]

Bismuth vanadate and sodium titanate particles. The size distributions of the $BiVO_4$ and $(Bi_{0.5}Na_{0.5})TiO_3$ particles are also presented in the ESI (Fig. S2†) and are very different from the monodisperse Au-core/Ag-shell particles. The median particle sizes estimated for these nanoparticles also deviated from the primary particle sizes as determined by SEM, regardless of the mass spectrometer used. Specifically, spICP-MS produced a spherical equivalent diameter in the range of 178 to 197 nm for $BiVO_4$ (primary particle size by SEM was 69 ± 23 nm), and 160–221 nm for $(Bi_{0.5}Na_{0.5})TiO_3$ (primary particle size by SEM was 106 ± 49 nm) (Table 1). These significant size differences between sp-ICP-MS and SEM cannot be explained by variabilities originating from the use of different techniques, but are a consequence of the presence of aggregates and/or agglomerates in the suspensions of these amorphous particles as observed with SEM analysis (ESI Fig. S1†) and as can be seen in the size distributions of the spICP-MS measurements (ESI Fig. S2†). sp-ICP-MS cannot distinguish primary particles from aggregates and agglomerates and returns a spherical equivalent size. The geometric particle size of typical $BiVO_4$ and $(Bi_{0.5}Na_{0.5})TiO_3$ aggregates/agglomerates as measured with SEM ranged from 200 to 800 nm. For loosely packed agglomerates (with a packing ratio of 0.2) this corresponds to spherical equivalent diameters in the range of 120 to 450 nm, comparable with the size ranges of the $BiVO_4$ and $(Bi_{0.5}Na_{0.5})TiO_3$ particles measured with spICP-MS.

In addition to particle sizing, with the icpTOF instrument we were able to monitor the signals of Ti and Bi (the signal of Na was below LOD) from $(Bi_{0.5}Na_{0.5})TiO_3$ NPs in a time-resolved manner and observed that the maximum of the Bi signals appeared with a delay of ~0 μs to 200 μs (Fig. 1A and B) from those of Ti (ESI Fig. S3†). These temporal shifts have already been reported in the literature and the hypothesis for their origin was proposed.[26] According to the hypothesis these shifts occur in the plasma and only for particles which traverse the plasma with a radial shift from the central axis and only for elements with different boiling points. Bi and Ti have indeed different boiling points of ~1560 °C and ~3290 °C, respectively. The differences in the ionization potentials and the technical design of ion optics may also contribute to the delay,[27] *e.g.*, long distance between the point of ion sampling and mass analyzer might cause ion separation in time, in a similar manner as it happens in the TOF instruments. The important practical point of this observation is that the processes occurring in the plasma chamber and ion optics are common to all ICP-MS instruments, regardless of the mass analyzer used, and as such, these temporal shifts, although not always observable and controlled, may further decrease the accuracy of single particle analysis in sequential ICP-QMS.

Nano-steel platelets. Using spICP-MS, the particle sizes (as spherical equivalent diameter, Table 1) of the platelets were found to be in the range of 200 to 2400 nm (ESI Fig. S2†), which is substantially larger than the primary particle sizes determined by SEM (*i.e.*, 197 ± 89 nm, ESI Fig. S1†). However, primary particle sizes of 60 to 1500 nm have been reported for this material and, as with bismuth vanadate and sodium titanate nanoparticles, the platelets appear to be present in the form of aggregates and/or agglomerates. The geometric sizes of the loosely packed aggregates/agglomerates as observed with SEM are in the range of 500 to 2000 nm corresponding to spherical equivalent diameters of 300 to 900 nm. Due to the limited mass range of the CyTOF® 2 (89 to 210 amu), it was not possible to use this instrument for the analysis of nano-steel.

3.2 Determination of particle number and mass concentration

Au-core/Ag-shell particles. Results obtained by the ICP-TOFMS and -QMS instruments for the particle number concentration of the Au/Ag 60 particles ranged from 5.0×10^9 to 1.7×10^{10} particles mL^{-1} while that for the Au/Ag 80 particles ranged from 3.2×10^9 to 5.5×10^9 particles mL^{-1}. On the average this is 73% and 82% of the particle number concentrations reported by the supplier (Table 2), if the results of the CyTOF® 2 are excluded. Recoveries of particle number concentration determined with spICP-MS are reported in the literature and range from 14% (Ag NP in chicken meat)[4] up to 73% (Ag NP in orange juice).[27] For the particle mass concentrations (Table 3) of the Au/Ag 60 (3 to 25 mg L^{-1}) and Au/Ag 80 (6 to 20 mg L^{-1}) particles, similar results are found. On the average, recoveries of 55–95% are found if the results of the CyTOF® 2 are excluded. Particle number and particle mass concentrations determined with the CyTOF® 2 were a factor 2–5 lower than the values reported by the supplier for both types of core/shell particles. In the CyTOF® 2 instrument the sample is introduced into the heated spray chamber by a flow injection

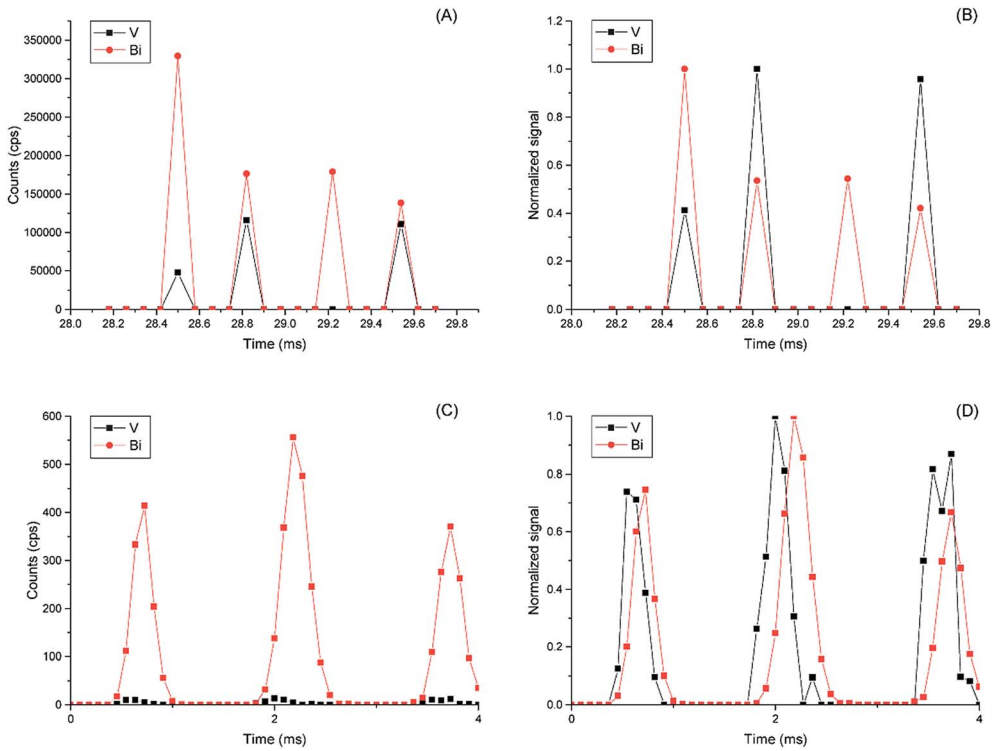

Fig. 1 Example of raw and normalized signals of $BiVO_4$ particles obtained by (A and B) quadrupole ICP-MS (NexION® 350D) and (C and D) ICP-TOFMS (icpTOF).

Table 2 Particle number concentrations determined by spICP-MS on individual elements ($n = 3$). Average of 3 independent runs is reported

Nanoparticle type	Supplied particle number conc. (particles mL^{-1})	Particle number conc. determined by spICP-MS (particles mL^{-1})			
		icpTOF	CyTOF® 2	NexION® 350D	iCAP™ Q
Au/Ag 60 nm	2.2×10^{10}	1.7×10^{10}[b]	5.0×10^{9}[b]	1.5×10^{10}[b]	1.6×10^{10}[b]
Au/Ag 80 nm	6.4×10^{9}	5.0×109[b]	3.2×10^{9}[b]	5.3×10^{9}[b]	5.5×10^{9}[b]
$BiVO_4$	3.3×10^{12}[a] 2.1×10^{11}[d]	3.1×10^{11}[b]	1.2×10^{10}[c]	2.6×10^{10}[b]	5.2×10^{10}[b]
$(Bi_{0.5}Na_{0.5})TiO_3$	1.1×10^{12}[a] 1.6×10^{11}[d]	1.3×10^{11}[b]	2.5×10^{10}[c]	5.4×10^{10}[b]	8.6×10^{10}[b]
Nano-steel (IRMM-383)	4.6×10^{10}[a] 6.7×10^{9}[d]	4.0×109[b]	—	2.0×10^{9}[b]	2.0×10^{9}[b]

[a] Calculated based on the mass concentration and primary particle size (SEM) of the prepared suspension. [b] Average of particle number concentrations measured for every individual element. [c] Average number concentration measured with bismuth only. [d] Particle number concentration after correction for the formation of aggregates/agglomerates (see text in the article).

system which uses a rinsing solution to push the sample forward. It may be possible that this rinsing solution diluted the sample. Another explanation is the transport efficiency of the heated spray chamber (which has no drain) that might have been lower than the specified 100% resulting in the observed underestimation of the particle mass and number concentrations.

Bismuth vanadate and sodium titanate particles. For the bismuth vanadate and sodium titanate nanoparticles the expected particle number concentration was calculated from the initial mass of material that was used to prepare the suspensions and the primary particle size determined by SEM ($BiVO_4$: 4 g L^{-1}; 3.3×10^{12} particles mL^{-1}; $(Bi_{0.5}Na_{0.5})TiO_3$: 4 g L^{-1}; 1.1×10^{12} particles mL^{-1}). The particle number concentrations determined by the different instruments were in the range of 1.2×10^{10} to 3.1×10^{11} particles mL^{-1} for $BiVO_4$, and 2.5×10^{10} to 1.3×10^{11} particles mL^{-1} for $(Bi_{0.5}Na_{0.5})TiO_3$ particles (Table 2). In both cases the deviation is more than a factor of 10 which can be explained by the presence of aggregates and/or agglomerates in the particle suspensions. The spherical equivalent particle sizes that were determined with spICP-MS are, on the average, 2.5 times larger than the primary particle size determined by SEM. Using sp-ICP-MS particle sizes for the calculation, the supplied particle number concentration becomes $2.5^3 \approx 15$

Table 3 Particle mass concentrations determined by spICP-MS of individual elements ($n = 3$)

Nanoparticle type	Supplied particle mass conc. (mg L^{-1})	Particle mass conc. determined by spICP-MS (mg L^{-1})			
		icpTOF	CyTOF® 2	NexION® 350D	iCAP™ Q
Au/Ag 60 nm					
Total	29	17[b]	3[b]	25[b]	16[b]
Au	6	6	1	12	5
Ag	23	11	2	13	11
Au/Ag 80 nm					
Total	21	15[b]	6[b]	20[b]	15[b]
Au	9	7	3	11	7
Ag	12	8	3	9	8
$BiVO_4$					
Calculated on Bi	4000[a]	1630	410	690	810
Calculated on V		1060	—	980	940
$(Bi_{0.5}Na_{0.5})TiO_3$					
Calculated on Bi	4000[a]	790	470	630	780
Calculated on Ti		550	—	660	970
Nano-steel (IRMM-383)					
Total	2500[a]	890[b]	—	340[b]	440[b]
Fe		570		220	400
Cr		180		60	17
Ni		120		50	16
Mo		20		10	4

[a] Calculated as sum of mass conc. determined for individual elements. [b] Material was weighed and suspended in house.

times lower. This has been calculated for each particle type and is presented as a "size corrected" supplied particle number concentration in Table 2. Differences in particle number concentrations are now reduced by a factor of 2–4 (except for the CyTOF 2 instrument). The particle mass concentrations of $BiVO_4$ and $(Bi_{0.5}Na_{0.5})TiO_3$ were calculated based on detected Bi and V, and Bi and Ti, respectively, and using eqn (2). Ideally, the two reported particle mass concentrations for each particle should be the same. In practice, the ratio between concentrations determined with two elements (V or Bi, Ti or Bi) ranges from 0.7 to 1.5. ESI Fig. S4† shows the molar ratios of V/Bi and Ti/Bi as determined with the icpTOF, which were in average close to ratios expected from the particle stoichiometry. The particle mass concentrations ranged from 690 mg L^{-1} to 1630 mg L^{-1} for $BiVO_4$ and from 550 mg L^{-1} to 970 mg L^{-1} for $(Bi_{0.5}Na_{0.5})TiO_3$ particles (Table 3), a factor of 3–8 or more lower than the expected particle mass concentration These lower particle mass concentrations may be the result of particle sedimentation. The fraction of small particles those signals fall below LOD is another contribution to the underestimation of particle mass and number concentrations. Interlaboratory exercises with spICP-MS have shown inaccuracies of up to 100% for particle number and particle mass concentrations.[26] As for the Au-core/Ag-shell particles, results for the CyTOF® 2 instrument are a factor 2–5 lower than for the other ICP-MS systems.

Nano-steel platelets. For nano-steel platelets the expected particle number concentration was calculated based on the initial mass of material used to prepare the suspensions and the primary particle size (2.5 g L^{-1}; 4.6×10^{10} particles mL^{-1}). The measured particle number concentrations ranged from 2.0×10^9 particles mL^{-1} to 4.0×10^9 particles mL^{-1}, while the mass concentration varied from 0.3 g L^{-1} to 0.9 g L^{-1} (Tables 2 and 3). The particle size measured with the spICP-MS systems is about 2 times larger than the estimated primary particle size. As a consequence, the observed particle number concentration is about $2^3 = 8$ times lower than expected. This has been calculated for each instrument and is presented as a "size corrected" particle number in Table 2. The reason for the underestimation of the particle mass by a factor >2 may be explained by the fact that the nano-steel platelets suspension shows a fast sedimentation.[17] The same explanation is applied for lower particle number concentrations observed.

Another explanation for the observed underestimation of particle masses would be that nano-steel platelets are not completely vaporized, atomized and ionized in the plasma. Dequeldre *et al.* have evaluated this problem by calculating the vaporization time for UO_2 particles as a function of particle size.[28] Assuming a residence time of the particle in the plasma of 10^{-4} s their calculations indicate that the upper particle size for UO_2 would be ~2000 nm. Aeschliman *et al.* used high-speed digital photography to study the vaporization of micrometer sized Y_2O_3 particles and reported that these were completely vaporized in the plasma.[29] Garcia *et al.* studied ICP particle vaporization of SiO_2 particles by measuring the intensities of silicon emission lines with different excitation energies.[30] Their measurements indicated that SiO_2 particles up to 2000 nm will be vaporized completely in the ICP plasma. Since the boiling point of SiO_2 (2230 °C) and UO_2 and Y_2O_3 (4300 °C) are comparable or higher than that of steel (range 1370–2750 °C), we assume that the nano-steel platelets used in this study are completely vaporized, atomized and ionized in the plasma and that the observed particle losses are due to fast sedimentation.

3.3 Limits of detection for particle size

In spICP-MS, the d_{LOD} depends on the fractions of the analyte in the nanoparticle, polyatomic or isobaric interferences,[15] and chemical and electronic noise. The d_{LOD} can also differ substantially when the particle is embedded in a complex matrix as demonstrated for Au and Ag NP in fruit juices[27] and chicken meat.[4] While d_{LOD} values are commonly calculated using a 3-sigma approach,[22] in this study d_{LOD} values are estimated based on the Poisson distribution of the background noise in the sample which is a more conservative approach and returns more realistic values (usually higher LODs) in case of a low number of counts in the background.[23]

Au-core/Ag-shell particles. For Au, a d_{LOD} of 7 nm was obtained with the CyTOF® 2 instrument (Table 4), a value that is smaller than reported in the literature (10 nm and 13–20 nm).[19,22] In the case of Ag, only the CyTOF® 2 was able to obtain a d_{LOD} of 13 nm reflecting the d_{LOD} reported by Lee *et al.*[22] The d_{LOD} reported by Lee were calculated using the 3-sigma

Table 4 d_{LOD} determined by spICP-MS measurements of individual elements compared to the values reported by Lee *et al.*[22] Reported LODs[24] (calculated using 3× sigma method) are listed in the table as size range including minimum and maximum values determined theoretically (based on elemental standards) and experimentally (based on measured nanoparticles)

Element	LODs reported by Lee *et al.*[24] (nm)	d_{LOD} determined by spICP-MS measurements (nm)			
		icpTOF	CyTOF® 2	NexION® 350D	iCAP™ Q
Au	13–20	18	7	16	8
Ag	13–20	28	13	22	15
Ti	75–90	37	—	35	35
$(Bi_{0.5}Na_{0.5})TiO_3$[a]		59	—	56	56
Bi	12–16	21	32	66	40
$BiVO_4$[b]		25	38	79	48
$(Bi_{0.5}Na_{0.5})TiO_3$[b]		27	42	86	52
V	39–72	35	—	57	56
$BiVO_4$[c]		63	—	103	101
Fe	55–120	51	—	128	187
Cr	42–71	61	—	86	55
Ni	35–42	39	—	56	58
Mo	31–39	30	—	20	14
Nano-steel[d]		60	—	150	220

[a] Calculated based on Ti. [b] Calculated based on Bi. [c] Calculated based on V. [d] Calculated based on Fe.

approach. The d_{LOD} of the icpTOF instrument for Ag and Au matched those previously reported, *i.e.* 28 nm and 18 nm, respectively.[6] The d_{LOD} values for Au achieved with the iCAP™ Q and NexION® 350D instruments were 8 and 16 nm respectively, and for Ag 15 and 22 nm, respectively. Note that lower d_{LOD} values may be achieved for Au with the NexION® 350D if a lower dwell time is used in the Syngistix™ Nano Application Module. The icpTOF instrument was tuned for the optimal sensitivity over the entire mass range, but can be optimized for Au and Ag only to improve their LODs.

Bismuth vanadate and sodium titanate particles. We report both d_{LOD} for composite particles and d_{LOD} for single element metallic particles composed of either Bi, Ti or V. All instruments achieved an average d_{LOD} for titanium metallic particle of 37 nm that was lower than previously reported values which were in the range of 75 to 90 nm,[23] and 50 nm for TiO_2 particles in food products.[20] This size translates into 59 nm d_{LOD} of bismuth titanate particle. The d_{LOD} for vanadium ranged from 35 nm (icpTOF) to 57 nm (NexION® 350D) which are comparable to earlier reported values.[22] These values translate into d_{LOD} of 63 nm (icpTOF) and 103 nm (NexION® 350D) for the bismuth vanadate particle. d_{LOD} values determined for bismuth were higher by a factor of 2 to 5 compared to the reported d_{LOD} value of 12 nm.[22] The d_{LOD} values obtained for bismuth ranged from 21 nm (icpTOF) to 66 nm (NexION® 350D). These higher d_{LOD} values resulted from a higher ionic background of bismuth. The d_{LOD} values translate into d_{LOD} values of 26 nm (icpTOF) and 83 nm (NexION® 350D) for the bismuth vanadate and sodium titanate particles. The d_{LOD} values explain the lower particle number concentrations found in suspensions of these materials (Table 2) since the higher d_{LOD} values (NexION® 350D) are close to the primary particle size of bismuth vanadate and sodium titanate particles.

Nano-steel platelets. The highest differences in estimated d_{LOD} between ICP-TOFMS and ICP-QMS instruments were observed for iron (Fe) (Table 4). This difference can be explained by the different collision and reaction cell operation modes that were used to compensate for interferences. In case of the icpTOF instrument (d_{LOD} Fe, 51 nm), hydrogen was used which neutralizes the interfering ArO^+, while helium was used in the kinetic energy dispersion (KED) mode in the ICP-QMS instruments resulting in d_{LOD} values for Fe of 128 nm (NexION® 350D) and 187 nm (iCAP™ Q).[31] As an alternative, the use of ammonia as reaction gas may improve the reported d_{LOD} for Fe in quadrupole instruments.[32] Furthermore, the icpTOF instrument was operated at a higher mass resolution enabling a partial separation of the analyte m/z peak and that of interferences. For pure nickel metallic particles (Ni), the estimated d_{LOD} values of 39 (icpTOF) to 58 nm (iCAP™ Q) exceed the values reported in the literature (35–42 nm)[22] (Table 4). d_{LOD} determined for chromium (Cr) and molybdenum (Mo) fall into the reported d_{LOD} range[22] or were lower, *i.e.* for Mo 20 nm with NexION® 350D and 14 nm with the iCAP™ Q instrument.

3.4 Multi-element capability

Au-core/Ag-shell particles. The average duration of a particle event, as determined by icpTOF, was 500 to 700 μs. The icpTOF instrument could simultaneously detect Au and Ag in 97% of particle events while the CyTOF® 2 instrument simultaneously detected both elements in 99% of all particle events. For the quadrupoles, which detected only 2 to 3 data points per particle event, the NexION® 350D was able to detect both elements in 55% (Au/Ag 60) and 66% (Au/Ag 80) of cases and outperformed the iCAP™ Q which detected both elements in 43 and 51% of cases (Table 5).

Bismuth vanadate and sodium titanate particles. For the $BiVO_4$ and $(Bi_{0.5}Na_{0.5})TiO_3$ particles, the time duration of one particle event, as determined by icpTOF, was between 600 to 800 μs (Fig. 1). The icpTOF detected two elements (Bi and V from $BiVO_4$ and Bi and Ti from $(Bi_{0.5}Na_{0.5})TiO_3$) in >90% of all particle events (the Na signal was below d_{LOD} for all particles) (Table 5). The NexION® 350D detected both elements in 72% ($BiVO_4$) and 68% ($(Bi_{0.5}Na_{0.5})TiO_3$) of all particle events, while the iCAP™ Q detected two elements in 42 and 55% of cases (Table 5). The differences between the TOFMS and QMS instruments can be explained by the fact that the QMS systems have dwell and settling times, while the TOFMS instruments measure everything simultaneously. In some particles, the amount of measured element was below the detection limit and, therefore, this element was not detected. This explains the incident detection of multiple elements to be <100%. In addition, the d_{LOD} values are better for the TOFMS instruments and the observed temporal shifts in the signals may further decrease the accuracy of the QMS instrument detection. The differences between the two QMS instruments could not be explained by

Table 5 Percentage of detected multi-element events within one particle obtained by spICP-MS. Average of 3 independent runs is reported

Nanoparticle type	Type of event	icpTOF	CyTOF® 2	NexION® 350D	iCAP™ Q
Au/Ag 60	2 Elements detected	98%	99%	55%	43%
Au/Ag 80	2 Elements detected	97%	97%	66%	51%
$BiVO_4$	2 Elements detected	92%	—	72%	42%
$(Bi_{0.5}Na_{0.5})TiO_3$	2 Elements detected	93%	—	68%	55%
Nano-steel	4 Elements detected	88%	—	5%	4%

the differences in settling times nor the differences in d_{LOD} for the observed elements.

Nano-steel platelets. For nano-steel, the time duration of one individual particle event in the icpTOF was in the range of 1.3 to 1.6 ms. This long particle signal duration is explained by increased diffusion of the ion cloud due to use of a reaction or collision gas. The icpTOF detected up to 15 data points per particle event (Fig. 2) while the ICP-QMS instruments were limited to 1 to 2 data points. Using the icpTOF instrument four elements (Fe, Cr, Ni and Mo) could be detected simultaneously in 88% of all particle events (Table 5) and the actual elemental composition of the nano-steel platelets could be accurately determined (Table 6). The elemental composition of every individual particle was calculated and the average of 2000 particles is reported. As expected, the simultaneous detection of four elements per particle event by the QMS instruments happens only infrequently, 4% for the iCAP™ Q and 5% for the NexION® 350D (Table 5). As a consequence the determination of the actual elemental composition of the nano-steel platelets is less accurate (Table 3). In the case of the QMS instruments the elemental composition was not calculated on the individual particle basis, but from the average of the detected element masses and represents an average of the entire population. The results show that the average elemental composition of a particle population can be determined with QMS, provided all

Table 6 Expected and determined mass fraction of 4 elements in a sample of nano-steel platelets. The error reported for the icpTOF is the standard deviation of 2000 individual particles. The error reported for QMS

		Determined fraction		
Element	Expected fraction	icpTOF	NexION® 350D	iCAP™ Q
Fe	67–72%	68 ± 5%	72 ± 4%	80 ± 4%
Cr	16–26%	17 ± 3%	19 ± 4%	14 ± 3%
Ni	10–14%	12 ± 3%	9 ± 1%	6 ± 1%
Mo	2–4%	2.2 ± 0.6%	1.2 ± 0.1%	0.8 ± 0.1%

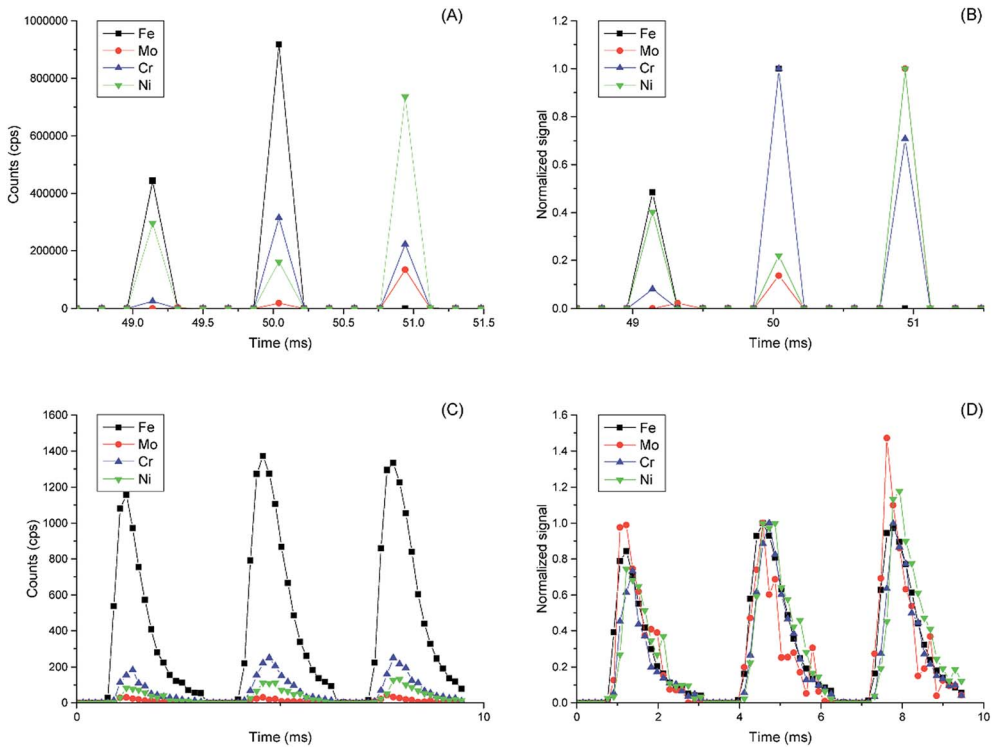

Fig. 2 Example of raw and normalized signals of nano-steel platelets obtained by (A and B) quadrupole ICP-MS (NexION® 350D) and (C and D) ICP-TOFMS (icpTOF).

particles have the same composition. Therefore, we conclude that the icpTOF can quantitatively detect a multiple number of elements within every particle without limitations or signal loss, while for quadrupole ICP-MS systems the multi-element detection is limited to two elements per particle and is rather qualitative. The ability to screen for multi-element NPs and to distinguish them from (multiple) single-element NPs is especially useful when dealing with unknown samples or differentiating between natural and engineered NPs.[33]

4. Concluding remarks

In this paper, we compared the performances of two ICP-TOFMS and two ICP-QMS instruments for the multi-element spICP-MS analysis of composite commercial NPs. Particle size results were comparable for both spICP-MS techniques. The substantial size differences with SEM were observed and explained by the presence of aggregates and/or agglomerates in the particle suspensions. In general, the spICP-TOFMS instruments showed smaller particle size detection limits (d_{LOD}) than the quadrupole instruments. For nano-steel, we demonstrated that spICP-TOFMS can quantitatively determine the composition of these multi-element nanoparticles without reducing the sensitivity when the number of elements increases, as it is the case for sequential QMS. spICP-TOFMS instruments showed true multiple-element capacity, however, the applicability of TOF instruments to determine the composition of real world samples has to be tested further and standardized methods for multi-element spICP-MS have to be developed. In contrast, QMS instruments are able to semi-quantitatively determine two elements in one particle. By further reduction of the instrument specific settling time and the use of shorter dwell times (<100 μs), improvement towards a multi-element detection may be possible. This is especially important since ICP-QMS instruments are, and will be, in use in many analytical laboratories.

Conflicts of interest

On behalf of all authors of this manuscript no conflict of interest exists.

Acknowledgements

The authors thank D. Kunkel from Charité – Universitätsmedizin Berlin (Germany) for the access to the CyTOF® 2 instrument. The authors are thankful to Thermo Fisher Scientific (Bremen, Germany) that provided the iCAP™ Q used in this study to RIKILT. In addition, the authors thank L. Boselli (University College Dublin) for providing of bismuth sodium titanate and vanadate particles. This study has received funding from the EMPIR program co-financed by the Participating States and from the European Union's Horizon 2020 research and innovation program within the InNanoPart (14IND12) EMPIR project. Furthermore, part of this work was funded by the European Union's Seventh Framework Program (FP7/2007–2013) project NanoDefine (grant agreement no. 604347).

References

1 ISO, *ISO/TS-19590: Nanotechnologies - Size distribution and concentration of inorganic nanoparticles in aqueous media via single particle inductively coupled plasma mass spectrometry*, Geneva, Switzerland, March 2017.
2 A. R. Montoro Bustos, E. J. Petersen, A. Possolo and M. R. Winchester, *Anal. Chem.*, 2015, **87**, 8809–8817.
3 R. J. Peters, H. Bouwmeester, S. Gottardo, V. Amenta, M. Arena, P. Brandhoff, H. J. Marvin, A. Mech, F. B. Moniz and L. Q. Pesudo, *Trends Food Sci. Technol.*, 2016, **54**, 155–164.
4 R. J. Peters, Z. H. Rivera, G. van Bemmel, H. J. Marvin, S. Weigel and H. Bouwmeester, *Anal. Bioanal. Chem.*, 2014, **406**, 3875–3885.
5 B. Nowack, M. Baalousha, N. Bornhöft, Q. Chaudhry, G. Cornelis, J. Cotterill, A. Gondikas, M. Hassellöv, J. Lead and D. M. Mitrano, *Environ. Sci.: Nano*, 2015, **2**, 421–428.
6 O. Borovinskaya, S. Gschwind, B. Hattendorf, M. Tanner and D. Günther, *Anal. Chem.*, 2014, **86**, 8142–8148.
7 M. Montano, H. Badiei, S. Bazargan and J. Ranville, *Environ. Sci.: Nano*, 2014, **1**, 338–346.
8 D. R. Bandura, V. I. Baranov, O. I. Ornatsky, A. Antonov, R. Kinach, X. Lou, S. Pavlov, S. Vorobiev, J. E. Dick and S. D. Tanner, *Anal. Chem.*, 2009, **81**, 6813–6822.
9 S. Becker. *Inorganic mass spectrometry: principles and applications*, John Wiley & Sons, New York, 2008.
10 A. Hineman and C. Stephan, *J. Anal. At. Spectrom.*, 2014, **29**, 1252–1257.
11 H. P. Longerich, S. E. Jackson and D. Günther, *J. Anal. At. Spectrom.*, 1996, **11**, 899–904.
12 R. C. Merrifield, C. Stephan and J. R. Lead, *Talanta*, 2016, **162**, 130–134.
13 J. Qi, L. Sun, P. Du and L. Li, *J. Am. Ceram. Soc.*, 2010, **93**, 1044–1048.
14 R. Strobel, H. J. Metz and S. E. Pratsinis, *Materials*, 2008, **20**, 6346–6351.
15 I. Kálomista, A. Kéri and G. Galbács, *J. Anal. At. Spectrom.*, 2016, **31**, 1112–1122.
16 J. Schindelin, I. Arganda-Carreras, E. Frise, V. Kaynig, M. Longair, T. Pietzsch, S. Preibisch, C. Rueden, S. Saalfeld, B. Schmid, J. Y. Tinevez, D. J. White, V. Hartenstein, K. Eliceiri, P. Tomancak and A. Cardona, *Nat. Methods*, 2012, **9**, 676–682.
17 D. Gilliland. *NanoDefine Technical Report D2.3. Standardised dispersion protocols for high priority materials groups*, 2016, available from, http://www.nanodefine.eu/publications/reports/NanoDefine_TechnicalReport_D2.3.pdf.
18 RIKILT, *Single Particle Calculation Tool*, 2016, available from, https://www.wageningenur.nl/en/show/Single-Particle-Calculation-tool.htm.
19 R. Peters, Z. Herrera-Rivera, A. Undas, M. van der Lee, H. Marvin, H. Bouwmeester and S. Weigel, *J. Anal. At. Spectrom.*, 2015, **30**, 1274–1285.
20 R. J. Peters, G. van Bemmel, Z. Herrera-Rivera, H. P. Helsper, H. J. Marvin, S. Weigel, P. C. Tromp, A. G. Oomen, A. G. Rietveld and H. Bouwmeester, *J. Agric. Food Chem.*, 2014, **62**, 6285–6293.

21 H. E. Pace, N. J. Rogers, C. Jarolimek, V. A. Coleman, C. P. Higgins and J. F. Ranville, *Anal. Chem.*, 2011, **83**, 9361–9369.
22 S. Lee, X. Bi, R. B. Reed, J. F. Ranville, P. Herckes and P. Westerhoff, *Environ. Sci. Technol.*, 2014, **48**, 10291–10300.
23 M. Tanner, *J. Anal. At. Spectrom.*, 2010, **25**, 405–407.
24 L. A. Currie, *Pure Appl. Chem.*, 1995, **67**, 1699–1723.
25 M. D. Montano, J. W. Olesik, A. G. Barber, K. Challis and J. F. Ranville, *Anal. Bioanal. Chem.*, 2016, **408**, 5053–5074.
26 O. Borovinskaya, M. Aghaei, L. Flamigni, B. Hattendorf, M. Tanner, A. Bogaerts and D. Günther, *J. Anal. At. Spectrom.*, 2014, **29**, 262–271.
27 M. Aghaei, H. Lindner and A. Bogaerts, *Anal. Chem.*, 2016, **88**, 8005–8018.
28 C. Degueldre, P. F. Favalger, R. Rossé and S. Wold, *Talanta*, 2006, **68**, 623–628.
29 D. B. Aeschliman, S. J. Bajic, D. P. Baldwin and R. S. Houk, *J. Anal. At. Spectrom.*, 2003, **18**, 1008–1014.
30 C. C. Garcia, A. Murtazin, S. Groh, V. Horvatic and K. Niemax, *J. Anal. At. Spectrom.*, 2010, **25**, 645–653.
31 N. I. Rousis, I. N. Pasias and N. S. Thomaidis, *Anal. Methods*, 2014, **6**, 5899–5908.
32 S. D. Tanner, V. I. Baranov and D. R. Bandura, *Spectrochim. Acta B Atom Spectrosc.*, 2002, **57**, 1361–1452.
33 A. Praetorius, A. Gundlach-Graham, E. Goldberg, W. Fabienke, J. Navratilova, A. Gondikas, R. Kaegi, D. Günther, T. Hofmann and F. van der Kammer, *Environ. Sci.: Nano*, 2017, **4**, 307–314.